COMPUTATIONAL STUDY OF LAMINAR FREE CONVECTION INSIDE TILTING IRREGULAR CAVITY OF A BATCH-TYPE SOLAR COLLECTOR

by

Fahad Sarfraz BUTT [a], ***Abdul Waheed BADAR*** [a*], ***Ajaz Bashir JANJUA*** [b], ***and Muhhamad Salman SIDDIQUI*** [c]

[a] Department of Mechanical Engineering, HITEC University, Taxila, Pakistan
[b] Design Shop, Heavy Mechanical Complex HMC, Taxila, Pakistan
[c] Faculty of Science and Technology, Norwegian University of Life Sciences, As, Norway

Original scientific paper
https://doi.org/10.2298/TSCI200521078B

Batch-type solar collector is a tilt-able water-heating solar-thermal system comprising an isosceles-trapezoidal enclosure housing a circular-cylinder absorber at the bottom wall, insulated side-walls, and flat-top glazing. Free convection of air inside such trapezoidal enclosure is studied numerically by varying the tilt angle of the whole enclosure from 0°-70°. The influence of tilt on the flow field has been demonstrated by plotting the streamlines and isotherms. The present study successfully identifies the importance of enclosure-tilt in quantifying heat-loss between absorber and glazing by developing a computational correlation between Nusselt and Rayleigh as a function of tilt. The correlation trend is non-monotonic over the range of angular Rayleigh numbers numerically experimented with having a peak around angular Rayleigh number $3 \cdot 10^5$ *corresponding to the tilt-angle 30°. The irregular-shaped cavity implies that the heat transfer correlations already existing for regular-shaped cavities may not be used otherwise they will draw implausible conclusions and this argument identifies the novelty of the present study.*

Key words*: batch-type solar collector, trapezoidal enclosure, Rayleigh number, free convection, tilt angle*

Introduction

Trapezoidal enclosure such as batch-type solar collector, fig. 1, also known as integrated-collector storage, is a simple and cost-effective device which essentially consists of a water storage-tank (circular-cylinder) that also acts as an absorber of the incident solar radiation [1]. It converts the solar energy directly into heat energy which is utilized to heat water for domestic usage. The cylinder containing working-fluid to be heated is housed in a trapezoidal enclosure whose top-surface is covered with flat glazing(s) and the remaining sides are insulated from the outside. The insides are layered with a reflecting material shaped as a flat or compound parabolic form to further enhance the amount of incident solar radiation on the absorber. Loss of heat from the heated cylinder to the outer glazing is by thermal radiation and by free convection of air. It is obvious that the performance of solar collectors is inversely proportional to the heat loss from the absorber.

* Corresponding author, e-mail: abdul.waheed@hitecuni.edu.pk

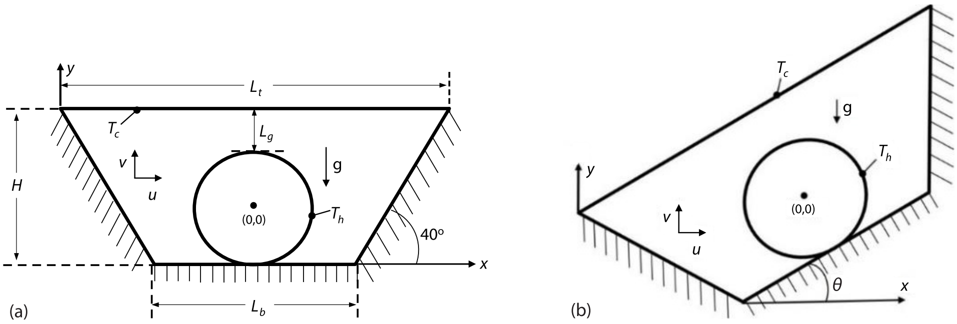

Figure 1. Schematic of the trapezoidal enclosure with heated cylinder at the bottom face; (a) simulated geometry and (b) tilted-view with tilt-angle θ

Different geographical regions would require dissimilar tilt-angles of the solar collector due to distinct solar incidence-angles to get maximum solar radiation. More or less loss of heat due to varying tilt-angles becomes the motivation of this research work. This may also imply that such solar collector will perform contrastingly in different geographical regions due to unequal tilt-angles even if the available global solar radiation and ambient conditions are same. Similar study is performed here that isolates the parametric effects of varying tilt-angles, $0° < \theta < 70°$, see fig. 1(b), in increments of 10°, on the convective heat transfer coefficient, h, in W/m^{2}K by fixing the temperature difference, ΔT, between absorber and thermal glazing. Following the nomenclature of Hollands *et al.* [2], it is interesting to represent Rayleigh number as Ra$\cos\theta$. Presented work employs laminar range: $1.38 \cdot 10^6 < \mathrm{Ra}\cos\theta < 4.03 \cdot 10^6$ with maximum Rayleigh number at zero tilt-angle.

It is pertinent to note that even though the enclosure is a regular isosceles-trapezoid, the cavity inside is not, as seen in fig. 1(a). Infact, it is complex and irregular due to the presence of circular-cylindrical inside. Accurate estimation of heat transfer due to free convection of air inside such irregular cavity is paramount to design and optimize the performance of such solar-thermal systems. Appropriate heat transfer correlations to predict the free convection of air inside such irregular cavities as a function of tilt-angles, gap-width between the absorber and glazing, *etc.*, are not available in the literature, to the best of authors' knowledge.

Any design-problem involving solar-thermal systems is usually accompanied by an array of unknowns (dimensions, angles) especially for geometries outside of the prevailing research trends. A heap of data exists for rectangular cavities but for irregular geometries as in fig. 1, one would be hard-pressed to find the literature of relevance. Notable experimental and numerical convective heat transfer studies in rectangular cavities are Catton and Edwards [3], Catton [4], Hollands *et al.* [2, 5], Ganzarolli and Milanez [6], Aydin [7], Sezai and Mohamad [8], Corcione [9], Sharif and Mohammad [10], Mahdavi *et al.* [11], Mehmoodi *et al.* [12], Mendu *et al.* [13], and Sourtiji and Hosseinizadeh [14]. To the best of authors' knowledge, no relevant study exists for our irregular geometry which has multiple applications in solar-thermal systems. One might be tempted to use existing heat transfer correlations but Singh and Eames [15] concluded their review that correlations developed for regular-shaped cavities can be misleading if applied to irregular cavities.

In fig. 1(a), gap-width between the top-most of the absorber-cylinder and successive glass-cover is an ambiguous yet important variable. Our work focuses on reducing convective losses from the absorber by finding the appropriate longitudinal tilt-angle as seen in fig. 1(b) Therefore, any gap-width will take the conductance out of the picture. Buchberg *et al.* [16] in their review paper recommended a gap-width range of 4-8 cm for minimum gap-convection. Their work, both theoretical and experimental, is based on rectangular cavities and is sensitive to ΔT. A rectangular cavity whether inclined or not has fixed gap-width across its entire length which is certainly not our case. Fixing an arbitrary gap-width equivalent to the radius of the absorber ($L_g = R \approx 0.15$ m) is selected for the current work in order to isolate parametric effects of tilt-angle on convective heat transfer. Side-walls are inclined at an angle of 40° with the horizontal. Longer of the two parallel lengths is $L_t \sim 1.55$ m and the shorter is $L_b \approx 0.46$ m whereas height is also $H \approx 0.46$ m.

Long debate can ensue on whether current study demands 2-D or 3-D analysis. Mallinson and de Vahl Davis [17] in their numerical study outlined two important results while examining 3-D convective heat transfer in a box: induction of axial velocity due to interaction of rotating fluid and stationary side-walls and thermal end-effects due to thermal-gradients normal to the side-walls. These effects especially the axial velocity caused the flow to be 3-D in the entire box. In an experimental work of Ozoe and Churchill [18], flow-dimensionality was attributed to thermal boundary-conditions. The 3-D roll-cells were observed in glycerine in square-cavities heated from below and conducting side-walls. The 2-D roll-cells were observed with insulated side-walls. In this irregular cavity study, side and bottom walls are non-conducting and insulated as well as uniformly heated on their entire surface-areas leading us to assume 2-Dity for all engineering estimates.

An inclined fluid-layer has peculiar heat transfer behavior. For small tilt-angles (from horizontal), flow is mostly buoyancy-driven and having longitudinal roll-cells but from a critical angle onwards to vertical, additional unstable stratification and thermal instabilities develop in the flow [19]. A useful literature review of free convection in inclined cavities is presented by Kolsi *et al.* [20]. compiling works of Koutsoheras and Charters [21], Talaie and Chen [22], Tzeng*et al.* [23], Skouta *et al.* [24], Ouriemi *et al.* [25], Bahi *et al.* [26], Alta and zen Kurtul [27], Skouta *et al.* [28], Jeng *et al.* [29], and Singh and Singh [30]. Most of these studies are numerical in nature, both steady and transient, spanning a range of Rayleigh, Nusselt, and Prandtl numbers, tilt-angle, aspect-ratio, thermal boundary-conditions, and with or without internal heat sources. All these studies voiced significant influence of tilt-angle on free convection and flow-development. Nevertheless, all these studies were conducted for regular cavities (square and rectangular).

Governing equations

Mass, momentum, and energy governing equations for incompressible buoyancy-driven flows are, respectively:

$$\frac{\partial u_i}{\partial x_i} = 0 \tag{1}$$

$$\rho u_j \frac{\partial u_i}{\partial x_i} = -\frac{\partial p}{\partial x_i} + \mu \frac{\partial^2 u_i}{\partial x_j^2} + \Delta\rho g_i \tag{2}$$

$$u_k \frac{\partial T}{\partial x_k} = \frac{k}{\rho c_p} \frac{\partial^2 T}{\partial x_j^2} \tag{3}$$

where dynamic viscosity, $\mu(T)$, density, $\rho(T)$, thermal-conductivity, $k(T)$, and specific heat at constant pressure, $c_p(T)$, are determined from thermodynamic property-tables, $\Delta\rho = -\rho\beta\Delta T$ is the Boussinesq approximation for the body-force term $g_i = (g_1, g_2) = (g\sin\theta, g\cos\theta)$, and β – the thermal expansion coefficient.

Equivalent non-dimensionalized forms are:

$$\frac{\partial \tilde{u}}{\partial \tilde{x}} + \frac{\partial \tilde{v}}{\partial \tilde{y}} = 0 \tag{4}$$

$$\tilde{u}\frac{\partial \tilde{u}}{\partial \tilde{x}} + \tilde{v}\frac{\partial \tilde{u}}{\partial \tilde{y}} = -\frac{\partial \tilde{p}}{\partial \tilde{x}} + \mathrm{Pr}\left(\frac{\partial^2 \tilde{u}}{\partial \tilde{x}^2} + \frac{\partial^2 \tilde{v}}{\partial \tilde{y}^2}\right) + \mathrm{RaPr}\tilde{T}\sin\theta \tag{5a}$$

$$\tilde{u}\frac{\partial \tilde{u}}{\partial \tilde{x}} + \tilde{v}\frac{\partial \tilde{v}}{\partial \tilde{y}} = -\frac{\partial \tilde{p}}{\partial \tilde{y}} + \mathrm{Pr}\left(\frac{\partial^2 \tilde{u}}{\partial \tilde{x}^2} + \frac{\partial^2 \tilde{v}}{\partial \tilde{y}^2}\right) + \mathrm{RaPr}\tilde{T}\cos\theta \tag{5b}$$

$$\tilde{u}\frac{\partial \tilde{T}}{\partial \tilde{t}} + \tilde{v}\frac{\partial \tilde{T}}{\partial \tilde{y}} = \frac{\partial^2 \tilde{T}}{\partial \tilde{x}^2} + \frac{\partial^2 \tilde{T}}{\partial \tilde{y}^2} \tag{6}$$

where Ra = $g\beta\Delta T L_g^3/(\nu\alpha)$ and Pr = ν/α are Rayleigh and Prandtl number, respectively, ν – momentum diffusivity, and α – thermal diffusivity. Rayleigh number can be viewed as a ratio of body-buoyancy forces to thermal and momentum forces. The aforementioned energy equation is written for zero pressure-gradient.

Computational set-up

Gmsh is employed for mesh generation. It is an open-source 3-D finite-element grid generator with a built-in CAD engine and post-processor [31]. The Code Saturne is utilized as a flow-solver which is also an open-source co-located finite-volume algorithm developed by Electricit´e de France able to handle unstructured meshes. Coding languages, extensive validation studies and the numerical methods used in Code Saturne are described in detail in Archambeau *et al.* [32]. It uses finite-volume method to discretize governing equations in space and time and a predictor-corrector approach is used for pressure-velocity coupling.

Transients are ignored since each numerical experiment mimics more or less the steady-state situation against an imposed ΔT. Radiative transport is trivialized and simulations are spatially 2-D utilizing symmetry in the depth of the trapezoidal enclosure at steady-states. Temperatures are uniformly distributed over the hot (absorber) and cold (top flat glazing) walls but the thermal flux shall vary along these walls in order to keep the temperature distribution uniform. Wall roughness effects are also excluded from the scheme of things.

Table 1 lists the numerical experiments performed in this study against a fixed ΔT of 20 K and Prandtl number of Pr = 0.71.

Table 1. Numerical experiments for Prandtl number of 0.71

θ Cases	T_h [K]	T_c [K]	T_{av} [K]	Racosθ
0°	343.15	323.15	333.15	$4.03 \cdot 10^6$
10°	343.15	323.15	333.15	$3.97 \cdot 10^6$
20°	343.15	323.15	333.15	$3.79 \cdot 10^6$
30°	343.15	323.15	333.15	$3.49 \cdot 10^6$
40°	343.15	323.15	333.15	$3.09 \cdot 10^6$
50°	343.15	323.15	333.15	$3.59 \cdot 10^6$
60°	343.15	323.15	333.15	$2.01 \cdot 10^6$
70°	343.15	323.15	333.15	$1.38 \cdot 10^6$

All numerical experiments are run using iterative treatment of the non-orthogonalities for determining the most-important gradient terms of the governing equations. Least-squares method for gradients is over-looked because the meshes used are not highly distorted. Pressure gradient in the governing equations is evaluated at each cell-center thereby requiring pressures at respective cell-faces which are generally obtained through standard centered interpolation. Pressure extrapolation domain boundaries is 1st-order Neumann. The Multigrid solver is used for pressure Poisson equation. The 2nd-order centered scheme is used for scalar velocities and a blend of SOLU (2nd-order linear upwind) and 1st-order upwind is used for advected scalar temperature. Diffusion terms in the governing equations are discretized using centered finite-difference formulation. Flux-reconstruction is used without slope-tests to account for mesh non-orthogonalities. Temperature based variation in thermodynamic properties is incorporated using user-defined programming. Uniform time-stepping is used to compute a steady-state solution which is also used for monitoring-points (fixed critical locations giving Eulerian information judge for true numerical convergence) output.

Mesh sensitivity study

Five meshes, Mesh-A, Mesh-B, Mesh-C, Mesh-D, and Mesh-E, were generated in Gmsh for $\theta = 0°$ each having 44390, 69192, 100490, 136422, and 179190 quadrangles, respectively. Mesh-E, on average, is four times denser compared to Mesh-A. All precautions were taken to obtain neat meshes. These were tested against two temperature differences, 11 K and 20 K to rule out thermal dependency. Each mesh was run for 8000 time-steps to obtain proper steady-state results. Figure 2 shows block-structured domain and the resultant structured-mesh in (x, y, z) and (x, y), respectively. Solver requires single-cell depth to run 2-D tests. Blocks were designed to obtain structured mesh with least skewing.

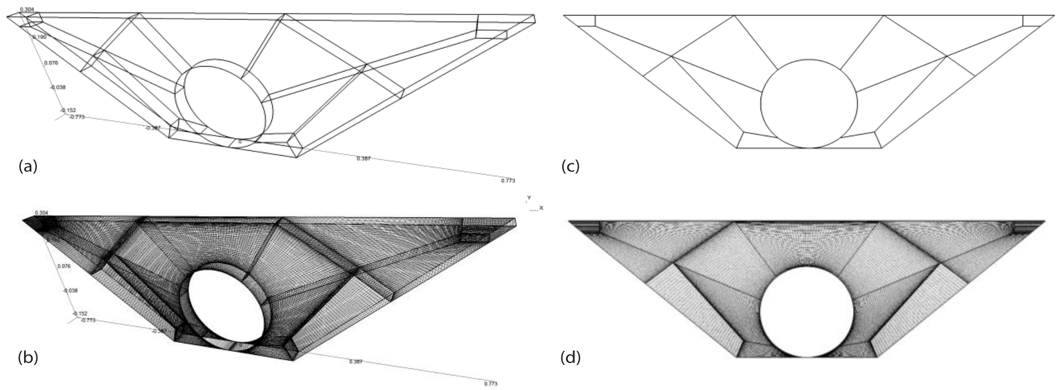

Figure 2. Control-volume mesh; (a) mesh-blocks in (x, y, z) (single-cell extrusion in z), (b) mesh-blocks in (x, v), (c) single-cell extruded mesh in (x, y, z), and (d) 2-D mesh in (x, y)

Boundary conditions are symmetry for the front and back walls, adiabatic (zero heat flux) Neumann boundary condition for the inclined side-walls and bottom-wall whereas imposed Dirichlet boundary conditions for the absorber and top flat glazing. Figures 3(a) and 3(b) demonstrate the diminishing trend of *h vs.* mesh-density slope. Considering the vanishing difference of h values between successive mesh pairs, Mesh-E has been selected for all numerical experiments. Any further increase in mesh-density is Boundary conditions are symmetry for the front and back walls, adiabatic (zero heat flux) Neumann boundary condition for the inclined side-walls and bottom-wall whereas imposed Dirichlet boundary conditions for the absorber and top flat glazing. Figures 3(a) and 3(b) demonstrate the diminishing trend of h *vs.* mesh-density slope. Considering the vanishing difference of h-values between successive mesh pairs, Mesh-E has been selected for all numerical experiments. Any further increase in mesh-density is unwarranted since the gain would be non-existent but the computational burden will be significantly increased. Mesh sensitivity study not only deals with the independence from mesh-density but also with the convergence, stability and steadiness of flow variables. The fluctuations due to initialization and spurious transients should either smooth out or settle-down around a mean to give a stable and steady profile. This is depicted for Mesh-E in fig. 3(c) which shows time-evolution (Eulerian history) of temperature at a fixed location of interest in the cavity. It shows the temperature profile oscillations are ± 0.25 K around the mean.

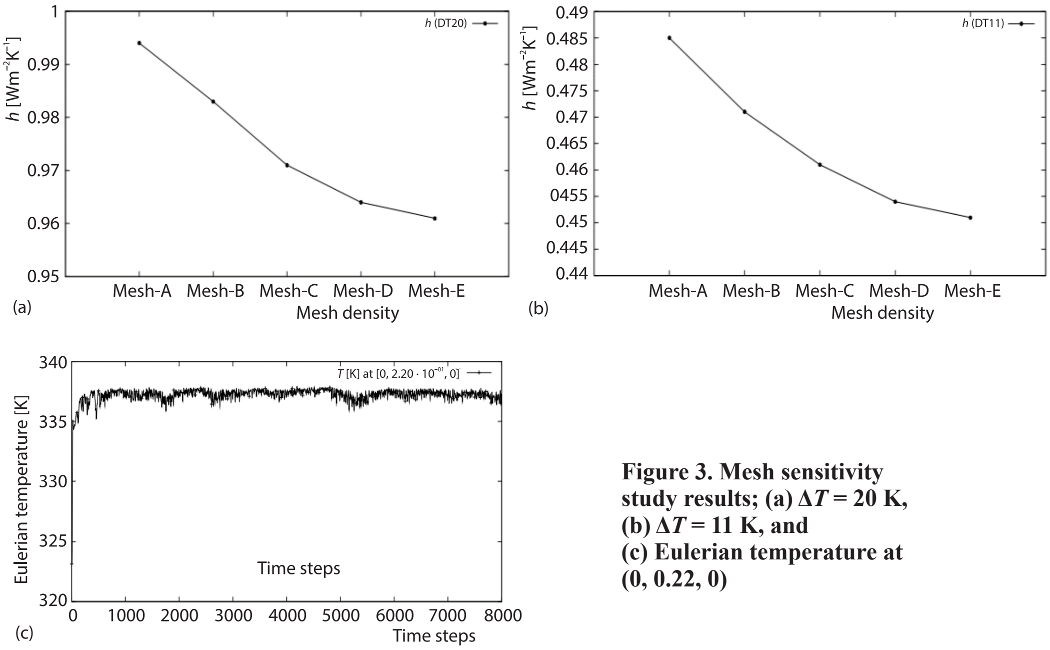

Figure 3. Mesh sensitivity study results; (a) ΔT = 20 K, (b) ΔT = 11 K, and (c) Eulerian temperature at (0, 0.22, 0)

Results and discussion

The steady-state results presented here are for $\Delta T = 20$ K demonstrating the effects of angular tilt on convection patterns in terms of streamlines of velocity magnitude $|V|$, iso-contours of normalized temperature: $T/|T_{\max}|$ and normalized velocities: $u/|u_{\max}|$, and $v/|v_{\max}|$, respectively, in x and y. Figures 4-7 represent streamlines, $u/|u_{max}|$, $v/|v_{\max}|$, and $T/|T_{max}|$, respectively, for $0° \leq \theta \leq 70°$ in increments of 10°. The variation in Nusselt number with angular Rayleigh is also presented and a correlation is suggested in this section.

Figure 4 show the streamlines of velocity magnitude $|V|$ for all tilt-angles. For the case of 0° the overall pattern of streamlines, in fig. 4(a), is quite symmetric on both sides of the hot absorber circular-cylinder: the fluid moves-up along the circumference culminating at the symmetric stagnation point and rises vertically to the flat top wall. The low pressure separated regions are identical on both sides of the hot absorber. Normalized velocity $v/|v_{\max}|$ representing vertical component is quite strong around and above this stagnation region as depicted in fig. 6(a). The fluid is divided into two symmetric halves about the stagnation region and moves along the top flat wall of the cavity as evident by the large magnitude of $u/|u_{\max}|$ in fig. 5(a).

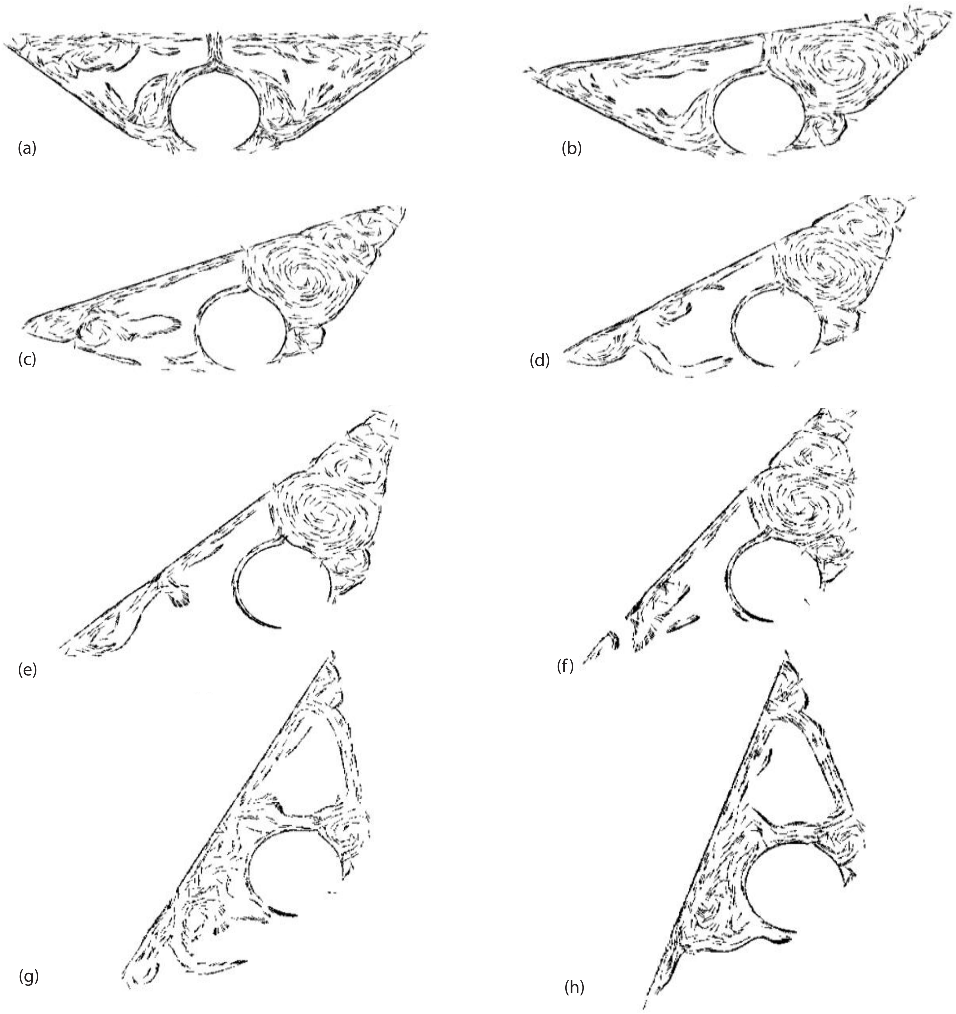

Figure 4. Streamlines of $|V|$ for $0° \leq \theta \leq 70°$; (a) $\theta = 0°$, (b) $\theta = 10°$, (c) $\theta = 20°$, (d) $\theta = 30°$, (e) $\theta = 40°$, (f) $\theta = 50°$, (g) $\theta = 60°$, and (h) $\theta = 70°$

The counter-rotating convections currents leave a sparse region adjacent to the absorber and as well as on the bottom and top corners. Iso-contours of $T/|T_{\max}|$ for 0° show similar behavio in fig. 7(a).

Increasing tilt-angle shifts the stagnation region clockwise on the hot absorber indicating the directional preference of convection, as evident in higher angle streamlines, normalized velocities and iso-contours of normalized temperature in all of the figures. For tilt-angle up-to 50°, the intensity of convection starts to shift to the upper right corner of the irregular cavity above the hot absorber. The clockwise and anti-clockwise rotation of the fluid in the form of one large and two-three small rolls is observed in this region while the flow separation occurs in front of and below the hot absorber. At tilt-angles of 60° and 70°, vortices are confined around the cylindrical hot absorber and near the walls of the irregular cavity which creates flow stagnant regions above and below the hot absorber.

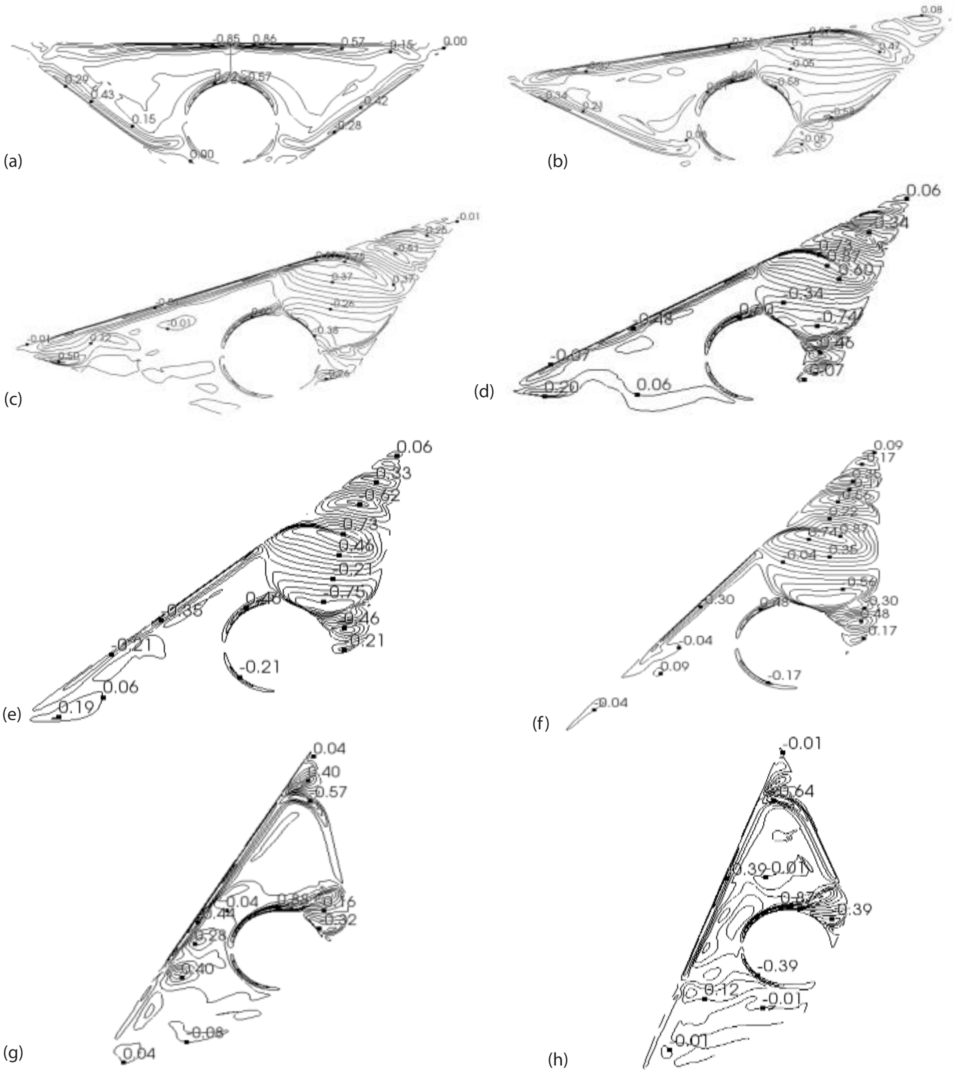

Figure 5. Isolines of $u/|u_{max}|$ for $0° \le \theta \le 70°$; (a) $\theta = 0°$, (b) $\theta = 10°$, (c) $\theta = 20°$, (d) $\theta = 30°$, (e) $\theta = 40°$, (f) $\theta = 50°$, (g) $\theta = 60°$, and (h) $\theta = 70°$

Normalized iso-contours $T/|T_{max}|$ in fig. 7 for 0° are symmetric on both sides of the hot absorber with respect to the vertical line separating the cavity into two halves. The symmetrical nature of $T/|T_{max}|$ iso-contours starts to deteriorate with an increase in tilt-angle. The curvatures of lines significantly increase from 0°-30° and then start to become more concentrated around the hot absorber from 40°-70°. It is also observed that the magnitudes of $T/|T_{max}|$ iso-contours remain well above 0.9 in the whole cavity thus indicating high air temperatures nearing the absorber temperature.

The heat transfer coefficients under steady-state are presented in terms of average Nusselt number. Figure 8(a) shows the variation of Nusselt number with respect to tilt-angle for the angular Rayleigh number, Racosθ. It can be seen that the variation in Nusselt number

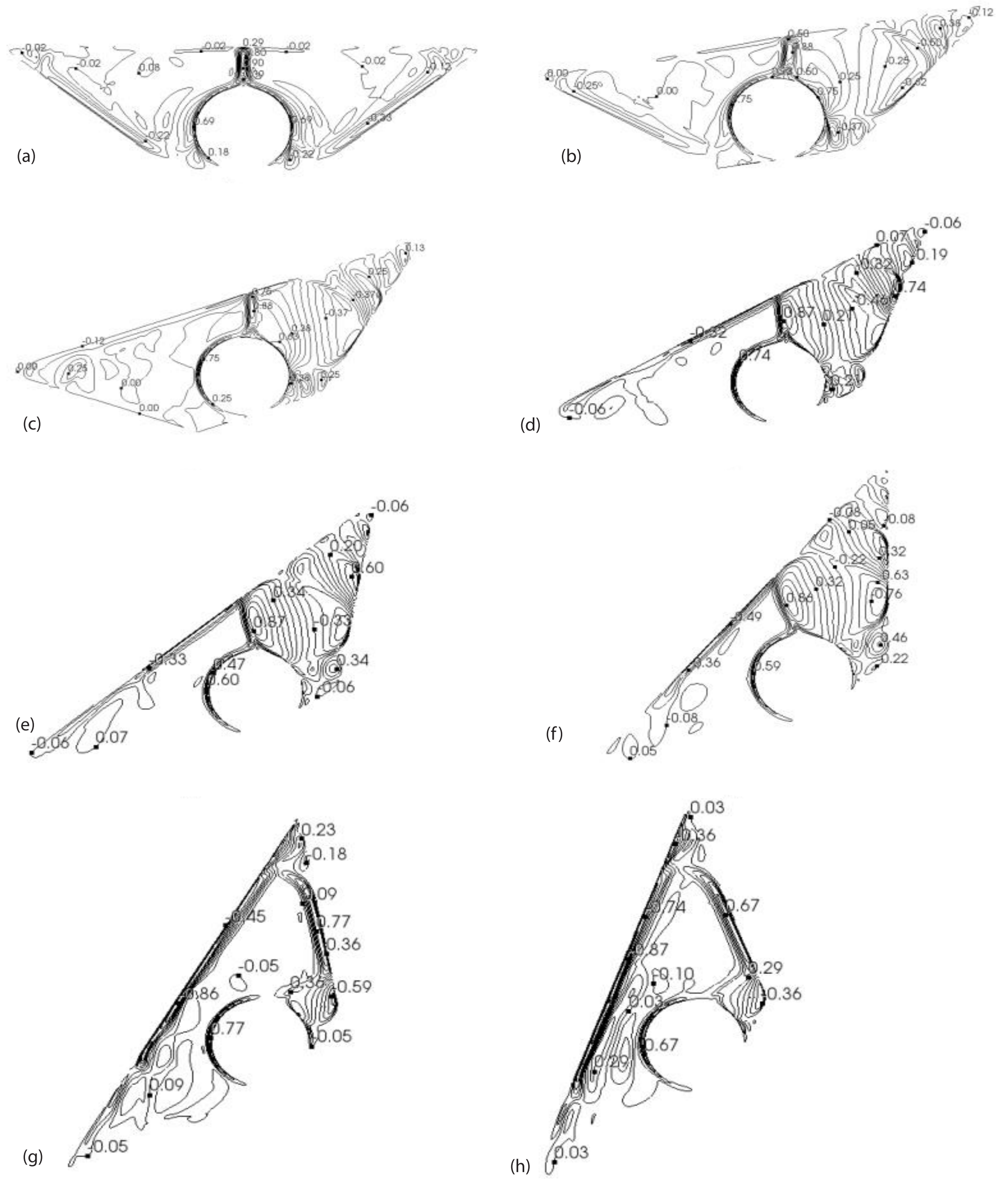

Figure 6. Isolines of $v/|v_{max}|$ for $0° \le \theta \le 70°$; (a) $\theta = 0°$, (b) $\theta = 10°$, (c) $\theta = 20°$, (d) $\theta = 30°$, (e) $\theta = 40°$, (f) $\theta = 50°$, (g) $\theta = 60°$, and (h) $\theta = 70°$

is mild for tilt-angles in the range of 0°-30° with peak-value occurs at 30^o due to the strong rolling motion of the fluid in the irregular cavity. The heat transfer rate then starts to drop with the increase in tilt-angle from 40°-70° and a significant drop in Nusselt number is observed at 60°. The irregular cavity is symmetric at zero-tilt having two identical patterns of counter-rotating convection currents on each side of the hot absorber. With a tilt of 10° the symmetricity is conveniently broken into two dissimilar patterns of convection currents having increased

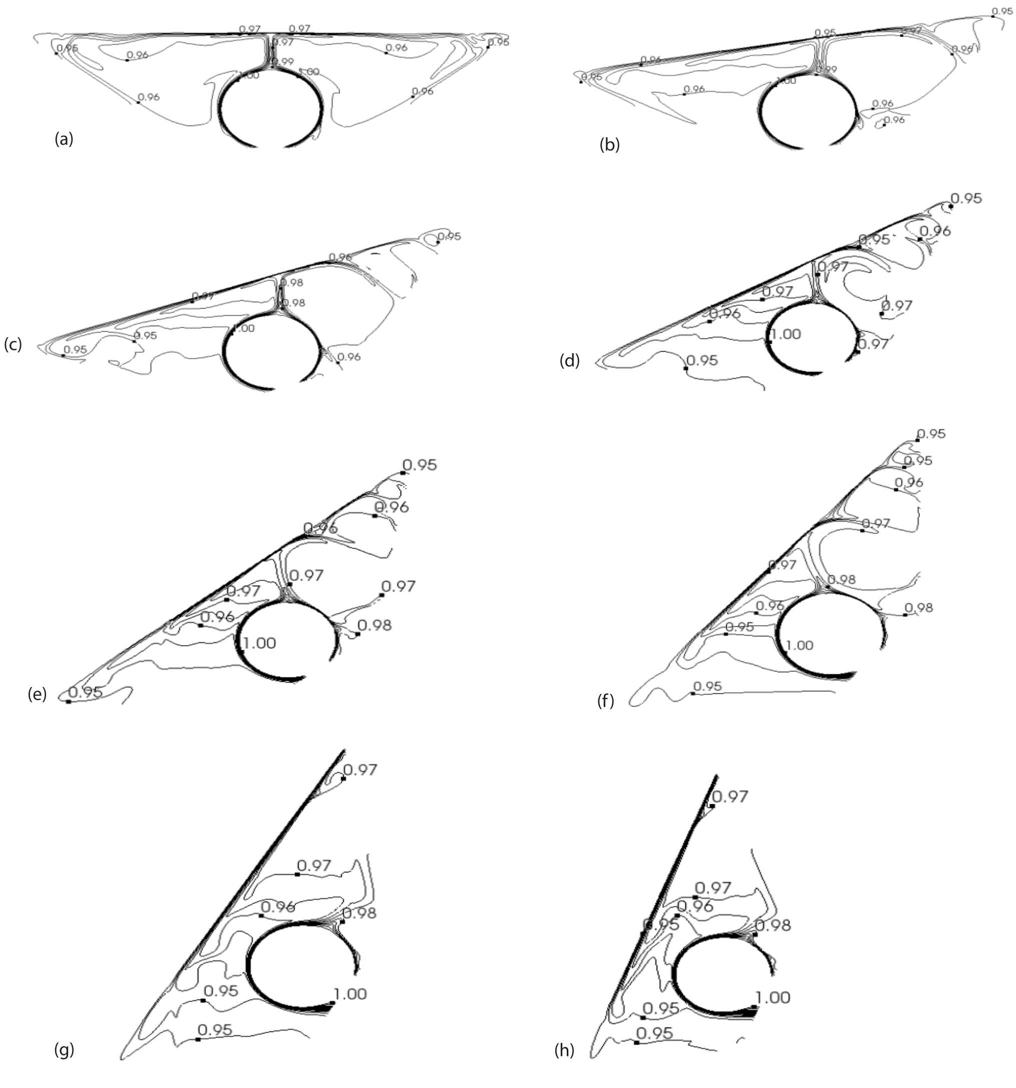

Figure 7. Isolines of $T/|T_{max}|$ for $0° \le \theta \le 70°$; (a) $\theta = 0°$, (b) $\theta = 10°$, (c) $\theta = 20°$, (d) $\theta = 30°$, (e) $\theta = 40°$, (f) $\theta = 50°$, (g) $\theta = 60°$, and (h) $\theta = 70°$

concentration and narrow rolls in the upper half of the cavity compared to the lower half where convection currents have larger rolls and sparse population. Due to the near-zero tilt, the lower half's significant yet little contribution the overall rate of heat transfer essentially highlights that the entire cavity-area is being utilized for heat transfer causing a drop in the overall Nusselt number. With a further increase in tilt, the effective heat transfer area shrinks to the upper half of the cavity despite the rate of heat release from the absorber is constant causing an increase in overall Nusselt number. This trend continues to around 30° where inflection point causes a decrease in the overall rate of heat transfer with a further increase in tilt.

Figure 8(b) depict Nusselt against angular Rayleigh variation and the following polynomial equation is developed to describe the relation between Nusselt number and Racosθ with R^2 coefficient of 0.99:

$$\begin{aligned}\mathrm{Nu} &= 2.44\cdot10^{-36}\left(\mathrm{Ra}\cos\theta\right)^6 - 4.14\cdot10^{-29}\left(\mathrm{Ra}\cos\theta\right)^5 + 2.86\cdot10^{-22}\left(\mathrm{Ra}\cos\theta\right)^4 - \\ &- 1.03\cdot10^{-15}\left(\mathrm{Ra}\cos\theta\right)^3 + 2.03\cdot10^{-0.9}\left(\mathrm{Ra}\cos\theta\right)^2 - 2.08\cdot10^{-0.3}\left(\mathrm{Ra}\cos\theta\right)^1 + 860.90\end{aligned} \tag{7}$$

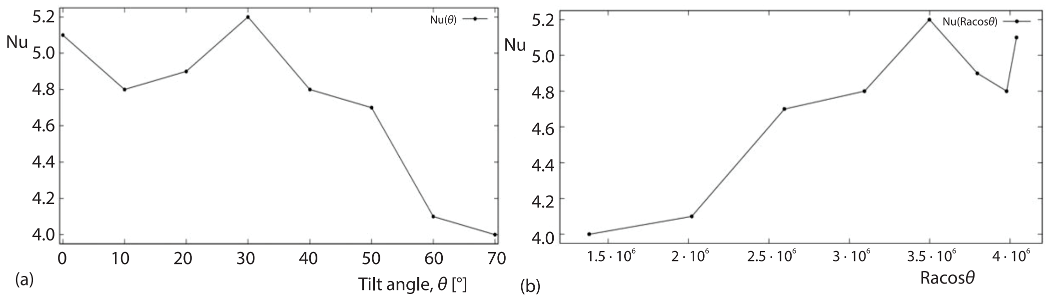

Figure 8. Nusselt number variations; (a) Nu *vs.* θ and (b) Nu *vs.* Racosθ

Natarajan *et al*. [33] used finite element analysis to investigate effect of bottom-wall heating on natural-convection in a cavity of trapezoidal shape. Results were presented for a range of Rayleigh and Prandtl numbers in the form of isotherms, stream functions and temperature profiles. The circulation patterns of Natarajan *et al*. [33] are qualitatively similar to the circulation patterns of no-tilt case of present work, fig. 4(a). The symmetricity of counter-rotating flow-circulation patterns can be qualitatively matched along with their densities and compressions. The effect of no-slip condition at the walls can also be matched by pointing out less circulation near the walls. This multi-cellular circulation is evident of the strong convection. A similar work of Basak *et al*. [34] studied bottom-wall heating effect on natural-convection in trapezoidal cavities. Results from finite element analysis are presented in the form of isotherms, stream functions and temperature profiles. Qualitative similarities of flow-patterns are quite evident here as well. Basak *et al*. [35] published another numerical work pertaining to natural-convection in trapezoidal enclosures by heating various walls of the cavity for a range of Rayleigh and Prandtl numbers. They observed flow-circulation symmetry when side-walls were linearly heated whereas in the present work side-walls are insulated; the similarity being that the side-walls are not differentially heated and the consequence is flow-symmetricity. In their second case which is linearly heated left-wall and cold right-wall, they have observed wavy patterns of local and average Nusselt numbers when plotted against Rayleigh for some values of Prandtl number in both simulated cases. In present-work, non-monotonic behaviour of Nusselt is also evident which is attributed to the presence of cold circular-cylinder at the bottom-wall of the trapezoid creating a cold-wall in addition insulated side-walls and heated top-wall. A comprehensive review published in 2016 by Das *et al*. [36] on natural-convection studies in non-square cavities also encapsulates these findings.

Conclusion

Numerical simulations are performed to study the influence of tilt angle on natural-convection heat transfer inside a trapezoidal cavity with a circular heating source placed at the bottom face. The tilt angle variation in the range of 0°-70° and the temperature difference of 20 °C are selected based on the most typical conditions and ranges encountered during the operation of such solar thermal collectors. It is concluded that the tilt-angles exercise considerable influence over the heat transfer performance of trapezoidal enclosures with the hot cylinder at the bottom edge especially for tilts upwards of 30° reducing Nusselt number monotonically until near-vertical tilt. It is also interesting to note that the Nusselt number *vs.* tilt-angle curve is non-monotonic for tilts downwards of 30° which is attributed to inflection-point of Nusselt number *vs.* θ curve between 20° and 30°. The rate of heat transfer decreases with the increasing tilt from 40°-70° and a substantial drop in Nusselt number is observed at 60°. A computational correlation is suggested which may be used accordingly to estimate the thermal performance of a batch-type solar collector, consisting of one cylinder placed inside a trapezoidal enclosure, at any tilt-angle between 0°-70°. The given correlation is valid for various ΔT conditions since the Rayleigh number is dependent on ΔT.

Nomenclature

g – acceleration due to gravity, [ms^{-2}]
H – gap-width between bottom-wall and flat-top glazing of the enclosure, [m]
h – free convection heat transfer coefficient, [Wm^{-2}K^{-1}]
L_b – length of the bottom wall of the enclosure, [m]
L_g – gap-width, [m]
L_t – length of the flat-top glazing of the enclosure, [m]
Nu – Nusselt number, [–]
Ra – Rayleigh number, [–]
Racosθ – angular Rayleigh number, [–]
T_{av} – average of T_c and T_h, [K]
T_c – cold-temperature of the flat-top glazing, [K]
T_h – hot-temperature of the absorber, [K]
ΔT – temperature difference between the absorber and flat-top glazing, [K]
T_{max} – steady-state maximum temperature of the cavity for each tilt, [K]
u – scalar velocity in x, [ms^{-1}]
u_{max}, v_{max} – steady-state maximum velocities of the cavity for each tilt, [ms^{-1}]
v – scalar velocity in y, [ms^{-1}]
x, y – co-ordinate axes in 2-D, [–]

Greek symbol

θ – tilt-angle of the enclosure with respect to horizontal, [°]

References

[1] Kalogirou, S. A., Solar Thermal Collectors and Applications, *Progress in Energy and Combustion Science*, *30* (2004), 3, pp. 231-295
[2] Hollands, K., *et al*., Free Convective Heat Transfer Across Inclined Air Layers, *ASME. J. Heat Transfer*, *98* (1976), 2, pp. 189-193
[3] Catton, I., Edwards, D., Effect of Side Walls on Natural-Convection between Horizontal Plates Heated from below, *ASME. J. Heat Transfer*, *89* (1967), 4, pp. 295-299
[4] Catton, I., Convection in a Closed Rectangular Region: The Onset of Motion, *ASME. J. Heat Transfer*, *92* (1970), 1, pp. 186-188
[5] Hollands, K., *et al*., Correlation Equations for Free Convection Heat Transfer in Horizontal Layers of Air and Water, *International Journal of Heat and Mass Transfer*, *18* (1975), 7, pp. 879-884
[6] Ganzarolli, M. M., Milanez, L. F., Natural-Convection in Rectangular Enclosures Heated from below and Symmetrically Cooled from the Sides, *International Journal of Heat and Mass Transfer*, *38* (1995), 6, pp. 1063-1073
[7] Aydin, O., Transient Natural-Convection in Rectangular Enclosures Heated from one Side and Cooled from above, *International Communications in Heat and Mass Transfer*, *26* (1999), 1, pp. 135-144
[8] Sezai, I., Mohamad, A., Natural-Convection from a Discrete Heat Source on the Bottom of a Horizontal Enclosure, *International Journal of Heat and Mass Transfer*, *43* (2000), 13, pp. 2257-2266
[9] Corcione, M., Effects of the Thermal Boundary Conditions at the Sidewalls Upon Natural-Convection in Rectangular Enclosures Heated from below and Cooled from above, *International Journal of Thermal Sciences*, *42* (2003), 2, pp. 199-208
[10] Sharif, M. A., Mohammad, T. R., Natural-Convection in Cavities with Constant Flux Heating at the Bottom Wall and Isothermal Cooling from the Sidewalls, *International Journal of Thermal Sciences*, (2005), 9, pp. 865-878
[11] Mahdavi, M., *et al*., Experimental and Numerical Study of the Thermal and Hydrodynamic Characteristics of Laminar Natural Convective Flow Inside a Rectangular Cavity with Water, Ethylene Glycolwater and Air, *Experimental Thermal and Fluid Science*, *78* (2016), May, pp. 50-64

[12] Mahmoodi, M., *et al*., Free Convection of a Nanofluid in a Square Cavity with a Heat Source on the Bottom Wall and Partially Cooled from Sides, *Thermal Science*, *18* (2014), Suppl. 2, pp. S283-S300
[13] Mendu, S. S, *et al*., Simulation of Natural-Convection of Nanofluids in a Square Enclosure Embedded with Bottom Discrete Heater, *Thermal Science*, *22* (2018), 6B, pp. 2771-2781
[14] Sourtiji, E., Hosseinizadeh, S. F., Heat Transfer Augmentation of Magnetohydrodynamics Natural-Convection in L-Shaped Cavities Utilizing Nanofluids, *Thermal Science*, *16* (2012), 2, pp. 489-501
[15] Singh, H., Eames, P. C., A Review of Natural Convective Heat Transfer Correlations in Rectangular Cross-Section Cavities and Their Potential Applications to Compound Parabolic Concentrating (CPC) Solar Collector Cavities, *Applied Thermal Engineering*, *31* (2011), 14-15, pp. 2186-2196
[16] Buchberg, H., *et al*., Natural-Convection in Enclosed Spacesa Review of Application Solar Energy Collection, *ASME, J. Heat Transfer*, *98* (1976), 2, pp. 182-188
[17] Mallinson, D., De Vahl Davis, G., The 3-D natural-Convection in a Box: A Numerical Study, *Journal of Fluid Mechanics*, *83* (1977), 1, pp. 1-31
[18] Ozoe, H., Churchill, S. W., Hydrodynamic Stability and Natural-Convection in Newtonian and Non-Newtonian Fluids Heated from below, C. E. P. Symposium Series No. 131 Heat Transfer: *Fundamentals and Industrial Applications*, *69* (1973), pp. 126-133
[19] Faghri, A., *et al*., *Advanced Heat and Mass Transfer*, Global Digital Press, Kanpur, India, 2010
[20] Kolsi, L., *et al*., A Comprehensive Review of Transient Natural-Convection Flow in Enclosures, *Journal of Basic and Applied Scientific Research*, *4* (2014), 11, pp. 17-24
[21] Koutsoheras, W., Charters, W., Natural-Convection Phenomena in Inclined Cells with Finite Side-Wallsa Numerical Solution, *Solar Energy*, *19* (1977), 5, pp. 433-438
[22] Talaie, V., Chen, C., Finite Analytic Solutions of Steady and Transient Natural-Convection in 2-D Rectangular Enclosures, *Proceedings*, ASME Winter Annual Meeting, Miami Beach, Fla., USA, 1985, Paper No. 85-WA/HT-68
[23] Tzeng, P. Y., *et al*., Numerical Investigation of Transient Flow-Mode Transition of Laminar Natural-Convection in an Inclined Enclosure, Numerical Heat Transfer – Part A: *Applications*, *31* (1997), 2, pp. 193-206
[24] Skouta, A., *et al*., Numerical Study of 2-D Transient Convection in an Air Filled Square Enclosure, Tilted in Relation the Horizontal Plane, Heated from Two Opposite Sides, *International Journal of Thermal Sciences*, *40* (2001), 4, pp. 352-365
[25] Ouriemi, M., *et al*., Natural-Convection of a Binary Fluid in a Slightly Inclined Shallow Cavity, Numerical Heat Transfer – Part A: *Applications*, *48* (2005), 6, pp. 547-565
[26] Bahi, A., *et al*., Natural-Convection in a Tilted Rectangular Enclosure with a Single Discrete Heater, *Journal of King Abdulaziz University: Engineering Sciences*, *16* (2005), 2, pp. 117-136
[27] Altac, Z., Kurtul, O., Natural-Convection in Tilted Rectangular Enclosures with a Vertically Situated Hot Plate Inside, *Applied Thermal Engineering*, *27* (2007), 11-12, pp. 1832-1840
[28] Skouta, R., *et al*., Numerical Study of the Transitionward Chaos of 2-D Natural-Convection Within in an Inclined Square Cavities, *Adv. Studies Theor. Phys*, *2* (2008), 1, pp. 37-50
[29] Jeng, D. Z., *et al*., Experimental and Numerical Study of Transient Natural-Convection Due to Mass Transfer in Inclined Enclosures, *International Journal of Heat and Mass Transfer*, *52* (2009), 1-2, pp. 181-192
[30] Singh, D. K., Singh, S. N., Combined Free Convection and Surface Radiation in Tilted Open Cavity, *International Journal of Thermal Sciences*, *107* (2016), Sept., pp. 111-120
[31] Geuzaine, C., *et al*., A 3-D Finite Element Mesh Generator with Built in pre- and post-Processing Facilities, *International Journal for Numerical Methods in Engineering*, *79* (2009), 11, pp. 1309-1331
[32] Archambeau, F., *et al*., Code Saturne: A Finite Volume Code for the Computation of Turbulent Incompressible Flows – Industrial Applications, *International Journal on Finite Volumes*, *1* (2004), 1
[33] Natarajan, E., *et al*., Natural-Convection Flows in a Trapezoidal Enclosure with Uniform and Non-Uniform Heating of Bottom Wall, *International Journal of Heat and Mass Transfer*, *51* (2008), 3-4, pp. 747-756
[34] Basak, T., *et al*., Heat Flow Analysis for Natural-Convection Within Trapezoidal Enclosures Based on Heatline Concept, *International Journal of Heat and Mass Transfer*, *52* (2009), 11, pp. 2471-2483
[35] Basak, T., *et al*., A Comprehensive Heatline Based Approach for Natural-Convection Flows in Trapezoidal Enclosures: Effect of Various Walls Heating, *International Journal of Thermal Sciences*, *50* (2011), 8, pp. 1385-1404
[36] Das, D., *et al*., Studies on Natural-Convection Within Enclosures of Various (Non-Square) Shapes – A Review, *International Journal of Heat and Mass Transfer*, *106* (2017), Mar., pp. 356-406

Paper submitted: May 21, 2020
Paper revised: February 3, 2021
Paper accepted: February 5, 2021